LETTER • OPEN ACCESS

Discharge mode conversion of bending flexible electrodes

To cite this article: Desheng Zhou *et al* 2024 *EPL* **145** 14002

A Letters Journal Exploring the Frontiers of Physics

January 2024

EPL, **145** (2023) 14002
doi: 10.1209/0295-5075/ad177c

www.epljournal.org

Discharge mode conversion of bending flexible electrodes

Desheng Zhou, Jiayin Li, Xin Tang[(a)] and Minkwan Kim[(b)]

University of Southampton - Southampton, SO17 1BJ, UK

received 17 October 2023; accepted in final form 20 December 2023
published online 7 February 2024

Abstract – Printed flexible electrodes have attracted widespread attention due to the low-cost process, large-area printing and resource saving. The performances of a flexible electrode in different applications is studied by researchers. In this paper, the characteristics of a flexible electrode with different bending angles are experimentally studied. Electrical, optical and productions characteristics are illustrated to demonstrate the performance of dielectric barrier discharge with a flexible electrode. Furthermore, the electrical fields are studied to explain the transfer of discharge mode and the corresponding discharge products.

Introduction. – Printed electronics technology is recently gathering attention as a novel method for fabricating electric circuits on a flexible board with metallic inks. It has the advantages of being low-cost process, having large-area printing and being resource saving. A considerable wide range of application fields of the printed electronics involves flexible integrated circuit, sensors, screen printing and so on [1]. The previous study also reported that electrodes printed by metallic ink generates DBDs could be generated on a complex curved surface in a large area by using printed electronics technology, broadening the application field of atmospheric pressure non-thermal plasma [2]. The corresponding printed electronics were also applied in the plasma flow control technique by Sato *et al.* which would expand the range of applications of DBD plasma actuators [3]. Besides, for the disinfection of curved surface, Weltmann *et al.* proposed a flexible electrode array arrangement, which would be applied in the complex 3D geometries [4]. Lu *et al.* also presented a flexible multi-pin plasma generator with movable electrodes, which would provide a large-area uniform plasma for the treatment of surfaces having different shapes [5]. Kim *et al.* reported an inkjet-printed flexible DBD source, which could significantly inhibit the growth of fungi on the surface of blueberries [6]. Gershman *et al.* demonstrated a combination of a flexible printed circuit design of a flex-DBD with H_2O_2 for surface decontamination from bacterial contaminants, which would result in a six-log reduction of bacterial load on a surface in 90 s [7].

The previous results demonstrate that flexible electrodes would be applied, for example, in flow control, disinfection and so on. They could adjust their shape according to different conditions. As a possible application environment, the bending of flexible electrodes could be applied in many specific scenarios, such as plasma generation in a non-flat surface [8–10]. However, a lot of research work has not been carried out on the characteristics of flexible electrodes under bending. In this paper, the characteristics of bended flexible electrodes are studied under different bending angles, the discharge images, U-I signals and corresponding ozone concentration are measured to demonstrate the discharge characteristics.

Experimental setup. – The discharge schematic is shown in fig. 1. A controllable AC power source is applied to generate high voltage, and a flexible DBD electrode is designed to generate plasma. The detail parameters are demonstrated in fig. 1. Current monitor (Pearson Model 6585, Pearson) and high-voltage probe (P6015A, Tektronix) are applied to measure the U-I signals. The discharge images are recorded using a digital single-lens reflex (DSLR) camera (Nikon D5600 with AS-F Micro NIKKOR 40 mm). Besides, the ozone concentration generated by DBD is measured by an ozone analyzer (49iQ, Thermo Fisher Scientific). The flexible electrode would be worked under different bending angles such as 0°, 60° and 180°, which is demonstrated in fig. 1(B). The golden wire

[(a)] E-mail: x.tang@soton.ac.uk
[(b)] E-mail: m.k.kim@soton.ac.uk (corresponding author)

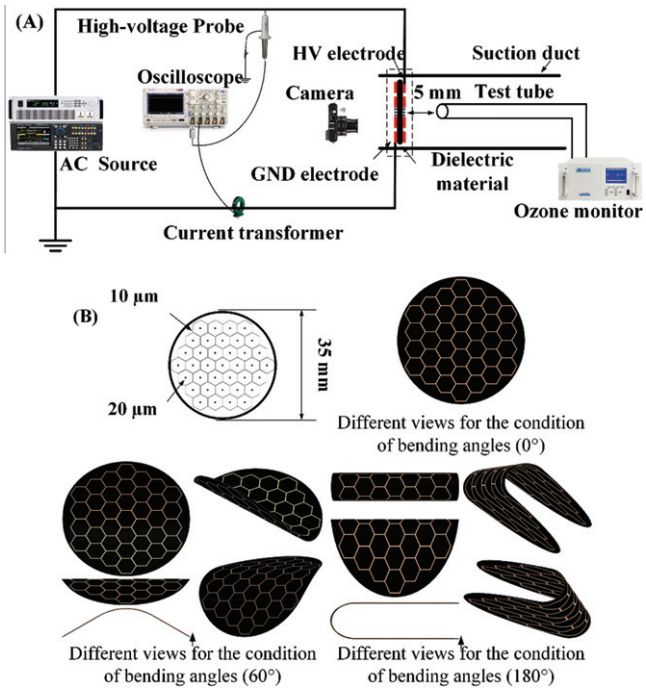

Fig. 1: Schematic of dielectric barrier discharge characteristics of a flexible electrode under different bending angles. (A) Experimental setup. (B) Different bending angles of the flexible electrode.

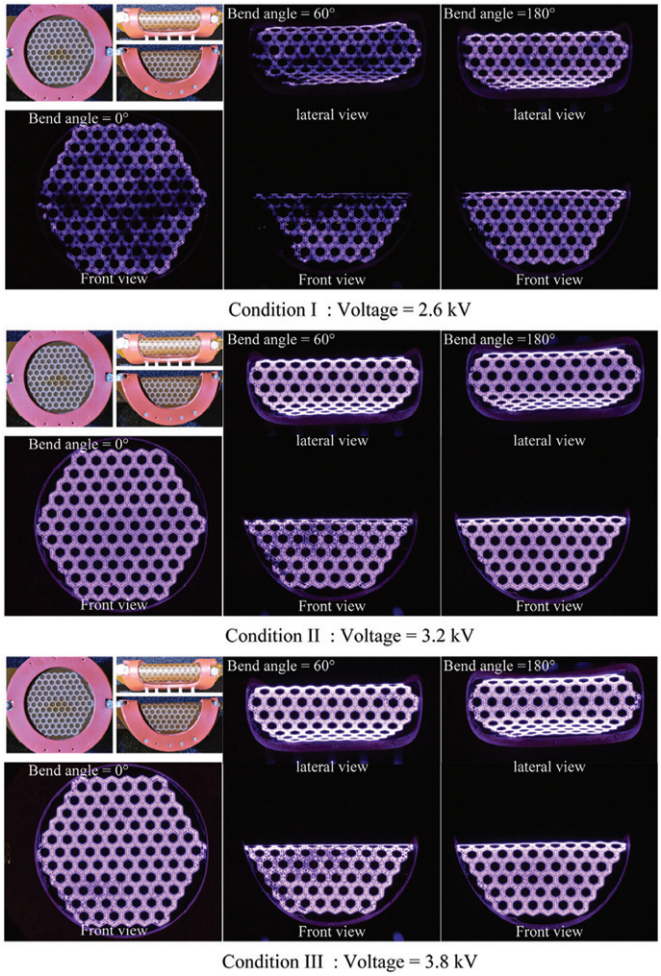

Fig. 2: Discharge images under different conditions (exposure time 1 second, ISO 3200, $f/6.3$).

represents the electrode, and the black part represents the insulating medium.

Results and discussions. – In this paper, three bending angles (0°, 60° and 180°, whose corresponding bending radii are infinity, 13 mm and 3 mm, respectively) are selected to measure the corresponding discharge characteristics, and two different perspective photos are taken under different input voltage. The DBD images under different curved angles are shown in fig. 2. For $U_{\mathrm{AC}} = 2.6\,\mathrm{kV}$, when the bending angle is 0°, the electrode is in a state of incomplete discharge, and the discharge color is blue-purple (during the transition of high-energy ions back to the ground state, blue-purple light is generated). By further increasing the bending angle to 180°, there is no obvious dark area in the overall discharge, and the light intensity has been improved visually. By further increasing the input voltage to 3.8 kV, when the curved angle is 0°, the discharge is uniform all over the electrode. and the overall appearance is blue-purple. When the curved angle is 60°, most parts of the discharge image is blue-purple, however, the discharge image in the bending area is white, and the luminous intensity of the discharge in some areas is dropped significantly. The discharge intensity is not uniform. When the bending angle is increased to 180°, the discharge intensity is further improved. The distribution of the discharge images under different conditions is demonstrated in fig. 3. The discharge images are employed grey scale processing and converted into spatial distribution states. The distribution and intensity of the discharge images under different conditions are much more obvious.

The U-I signals under different conditions are shown in fig. 4 (The bright blue curve is the voltage, and the sky blue, red and black curves represent the discharge current under different bending angles). For the input voltage of 2.6 kV, when the bending angle is 0°, there is almost no pulse in the current signal, and the discharge is similar in the corona state. By increasing the bending angle, the number and amplitude of current pulses are increased. When the input voltage is increased to $U_{\mathrm{AC}} = 3.8\,\mathrm{kV}$, the discharge pulses are significantly enhanced, and the discharge signals under the three bending angles also show obvious differences. For the bending angle 0°, the amplitude of the current pulse is about 5 mA, and for the bending angle 180°, the current amplitude is about 8 mA. There is a significant enhancement in the discharge intensity with increasing bending angle.

Furthermore, the ozone concentration is as a method for characterizing discharge products under different bending angle conditions. As can be seen in fig. 5, the

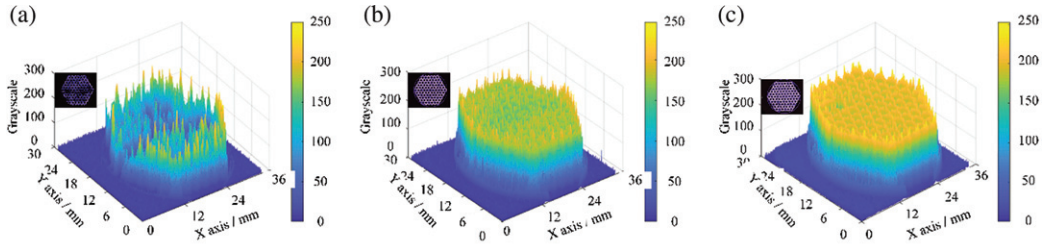

Distribution of discharge images under different input voltages for front view of bending angle 0°. (a) Voltage = 2.6 kV, (b) voltage = 3.2 kV, (c) voltage = 3.8 kV.

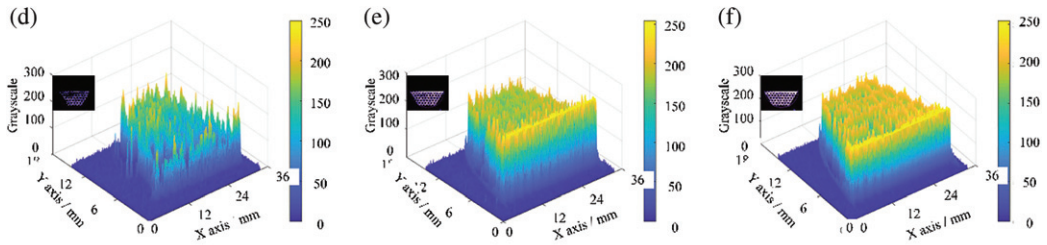

Distribution of discharge images under different input voltages for front view of bending angle 60°. (d) Voltage = 2.6 kV, (e) voltage = 3.2 kV, (f) voltage = 3.8 kV.

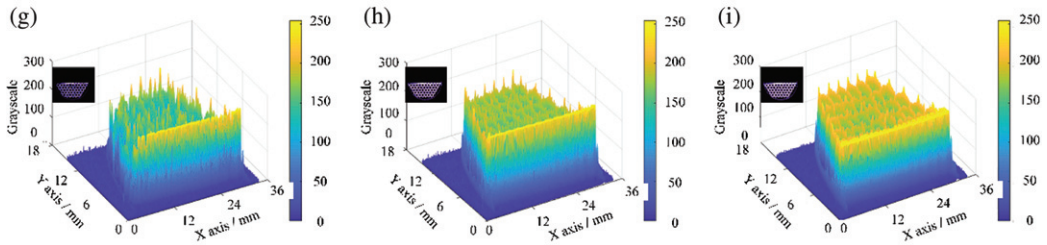

Distribution of discharge images under different input voltages for front view of bending angle 180°. (g) Voltage = 2.6 kV, (h) voltage = 3.2 kV, (i) voltage = 3.8 kV.

Fig. 3: Distribution of discharge images under different conditions for frond view.

concentration of ozone is shown with a monotonously increasing trend for the bending angles of 0° and 60°. The concentration is increased from 400 ppb to 2500 ppb when the input voltage increases by about 1.2 kV for the bending angle of 0°. For the bending angle of 60°, the value is about 1600 ppb for $U_{AC} = 3.8$ kV. However, when the bending angle is 180°, the ozone concentration would increase when the input voltage is less than 3.2 kV. By further increasing the input voltage, the ozone concentration is dropped due to the transfer of the discharge mode. For the input voltage of 3.8 kV, the concentration of ozone is about 320 ppb, which is about one-sixth for the condition of bending angle 0°.

Due to the mechanism of SDBD, the performance would be influenced by the electric field [10–13]. When the electrodes are not bent, the overall space electric field presents a uniform distribution state. By increasing the bending angle, the bending radius decreases, the concentration of the local electric-field distribution in the space would be enhanced, which would cause the discharge mode conversion [14–16]. The electric-field simulation of the bent electrode under different angles is shown in fig. 6.

As shown in fig. 5, when the bending angle is 0°, the maximum field strength is about 64.1 kV/mm, and when the bending angle is 60°, the field strength is increased by about 50%, and the maximum field strength is about 90.27 kV/mm (see also table 1). The bending electrode would obtain a higher electric-field strength for the same input voltage. As shown in fig. 2, under a larger bending angle, the discharge is more likely to occur.

The enhancement of the partial discharge would further increase the electrode surface temperature, especially the discharge mode is transferred from diffuse mode to filamentary mode. According to refs. [17–22], the concentration of ozone generated would be affected by the electrode temperature. With the increase of the electrode temperature, the ozone generation rate of reaction (formula (1)) decreased while the ozone decomposition rate following

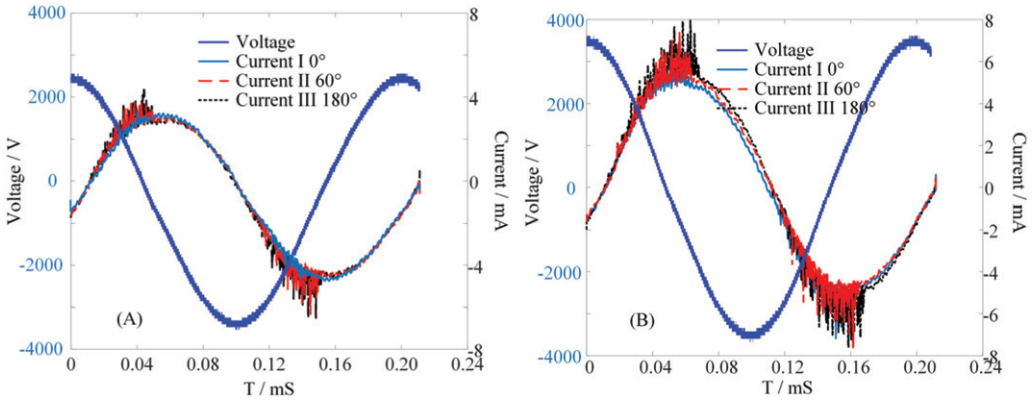

Fig. 4: U-I signals under different conditions for different input voltage: (a) $U_{\mathrm{pp}} = 2.6\,\mathrm{kV}$, (b) $U_{\mathrm{pp}} = 3.8\,\mathrm{kV}$.

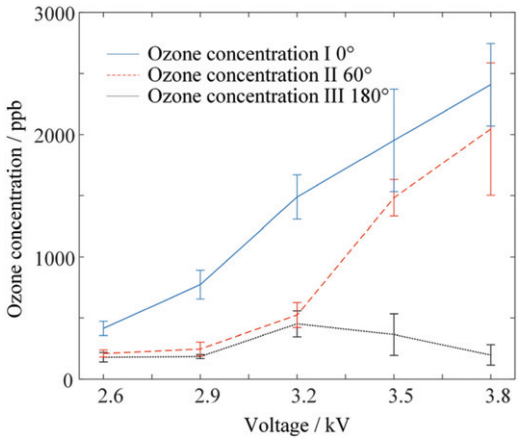

Fig. 5: Ozone concentration under different conditions.

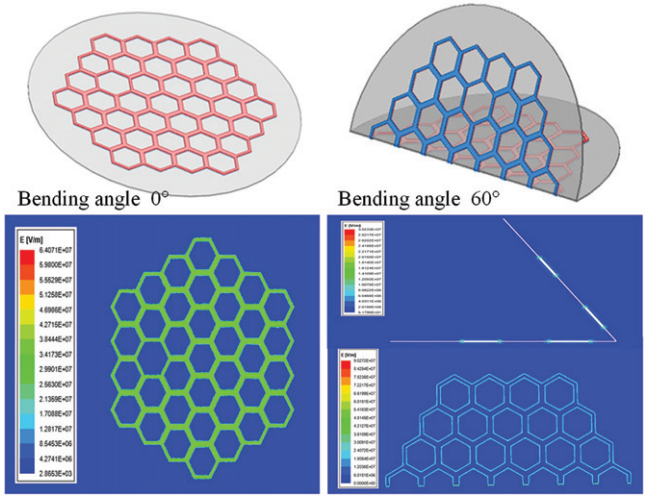

Fig. 6: Electric-field distribution of a flexible electrode under different bending angles.

reactions increases:

$$\mathrm{O}(^3\mathrm{P}) + \mathrm{O}_2 + \mathrm{M} \rightarrow \mathrm{O}_3 + \mathrm{M}. \tag{1}$$

Furthermore, two catalytic reaction cycles would lead to O_3 destruction and catalytic recombination of atomic oxygen (formulas (2), (3)). This would lead to decreasing ozone concentration with increasing electrode temperature,

$$\mathrm{NO} + \mathrm{O}_3 \rightarrow \mathrm{NO}_2 + \mathrm{O}_2, \tag{2}$$

$$\mathrm{NO}_2 + \mathrm{O} \rightarrow \mathrm{NO} + \mathrm{O}_2. \tag{3}$$

Table 1: Electric-field intensity under different bending angles. (Input voltage: 3.5 kV.)

Different bending angle	0°	60°
Maximum field strength (kV/mm)	64.1	90.27

Conclusion. – In summary, the characteristics of flexible electrode discharge are studied under different bending angles. The change of the space electric-field distribution caused by electrode bending would be the main reason for the discharge mode transfer and the concentration change of the oxygen generation.

* * *

This work is sponsored by the UK Space Agency (UKSAG22_ESE01 and UKSAG22_0006).

Data availability statement: All data that support the findings of this study are included within the article (and any supplementary files).

REFERENCES

[1] Guo Y. T., Fang M. Q., Zhang L. Y., Sun J. J., Wang X. X., Tie J. F., Zhou Q., Zhang L. Q. and Luo H. Y., *Appl. Phys. Lett.*, **121** (2022) 074101.
[2] Henrike H. and Kim M. K., *Plasma Res. Express*, **2** (2020) 035010.
[3] Sato S., Enokido T., Ashikawa K., Matsubara M., Kanie K. and Ohnishi N., *Sens. Actuators A: Phys*, **330** (2021) 112833.

[4] Weltmann K., Fricke K., Stieber M., Brandenburg R., von Woedtke T. and Schnabel U., *IEEE Trans. Plasma Sci.*, **40** (2012) 2963.
[5] Liu B., Qi F., Zhou D., Nie L., Xian Y. and Lu X., *Plasma Sci. Technol.*, **24** (2022) 035403.
[6] Kim D. J., Park J. and Han J. G., *Jpn. J. Appl. Phys.*, **55** (2016) 085102.
[7] Gershman S., Harreguy M. B., Yatom S., Raitses Y., Efthimion P. and Haspel G., *Sci. Rep.*, **11** (2021) 4626.
[8] Heo Y. S., Yim D. G., Baek K. H., Kang T., Lee Y. E., Kin J., Choe W. and Jo C., *Food Sci. Technol.*, **143** (2021) 111128.
[9] Park H. W., Cho I. J., Choi S. and Wha D., *IEEE Trans. Plasma Sci.*, **42** (2014) 2364.
[10] Homola T., Prukner V., Hoffer P. and Simek M., *Plasma Sources Sci. Technol.*, **29** (2020) 095014.
[11] Hao Y. P., Han Y. Y., Huang Z. M., Yang L., Dai D. and Li L. C., *Phys. Plasma*, **25** (2018) 013516.
[12] Kim J. H., Park J. S., Shin Y. S. and Kim C. K., *Korean J. Chem. Eng.*, **36** (2019) 1371.
[13] Peng B. F., Jiang N., Shang K. F., Lu N., Li J. and Wu Y., *High Voltage*, **7** (2022) 730.
[14] Zhu Z. Z., Zhang M. Y., Wang L. G., Zhang J. Y., Luo S. T., Wang Z. F., Guo L., Liu Z. J., Liu D. X. and Rong M. Z., *J. Phys. D. Appl. Phys.*, **56** (2023) 355201.
[15] Sun Y. Z., Zeng M. and Cui Z. Y., *Jpn. J. Appl. Phys.*, **51** (2012) 952.
[16] Yao J. X., Miao J. S., Li J. X. and Ouyang J. T., *Appl. Phys. Lett.*, **122** (2023) 082905.
[17] Xi W., Luo S. T., Liu D. X., Wang Z. F., Liu Z. J., Guo L., Wang X. H. and Rong M. Z., *Phys. Plasmas*, **29** (2022) 090701.
[18] Yuan D. K., Zhang G. X., Ling Z. Q., Wu A. J., He Y. and Wang Z. H., *Vacuum*, **176** (2020) 109351.
[19] Wei L. S., Xu M. and Zhang Y. F., *Ozone Sci. Eng.*, **41** (2019) 437.
[20] Pekarek S. and Mikes J., *Eur. Phys. J. D*, **68** (2014) 10.
[21] Jodzis S. and Baran K., *Vacuum*, **195** (2022) 110647.
[22] Mikes J., Pekarek S. and Soukup I., *J. Appl. Phys.*, **120** (2016) 17.